Programmable complex pumping field induced color-on-demand random lasing in fiber-integrated microbelts for speckle free imaging

Xiaoyu Shi[1], Kaiyue Shen[1], Yaoxing Bian[2], Wanting Song[1], Jun Ruan[1], Zhaona Wang[2] and Tianrui Zhai[1]*
1 College of Physics and Optoelectronics, Faculty of Science, Beijing University of Technology, Beijing 100124, China.
2 Applied Optics Beijing Area Major Laboratory, Department of Physics , Beijing Normal University, Beijing 100875, China,.
*trzhai@bjut.edu.cn

A: Calculation of the energy transfer efficiency

B: Waveguide integrated RLs with different gain and scattering parameter

C: Effect of the width of microbelt on the waveguide integrated RLs

D: Spatial coherence of the waveguide integrated RLs

E: Effect of the diameter of waveguide on the waveguide integrated RLs

F: Effect of the adjacent RL microbelts on a shared waveguide

G: Waveguide integrated RLs with different gain and scattering parameter

H: Imaging property under the illumination of RLs on fiber

A: Calculation of the energy transfer efficiency

The energy transfer coefficient is defined as

$$\eta_{\mathrm{RET}} = \frac{I_A}{I_A + I_B}$$

Figure R2a shows the fluorescence spectrum of the green and red fluorescent dyes that are pumped under a 355 nm pulsed laser. The energy transfer coefficient of the RL-G system is estimated as 0.85. In the same way, according to the fluorescence spectrum in Figure R2b, the energy transfer coefficient between S420 and RhB is estimated as 0.89 for the RL-R system.

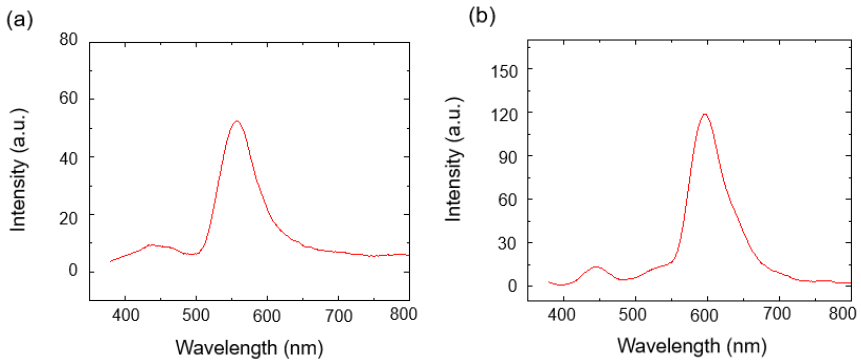

Figure S1. (a) Fluorescence spectra of the RL-G system. (b) Fluorescence spectra of the RL-R system. The excitation source is a pulsed laser at 355 nm.

B: Waveguide integrated RLs with different gain and scattering parameter

The influence of the scatterer concentration on waveguide integrated RLs have been presented in Figure S2a. The concentration of TiO_2 NPs in the mixed PVA solution (15wt%) is changed from 0.1 mg mL^{-1} to 4.8 mg mL^{-1} while keeping the concentration of Rhodamine 6G (R6G) at a fixed value of 1 mg mL^{-1}. When the concentration of TiO_2 NPs increases, the spectrum exhibits several sharp spikes blue shifts, as is displayed in Figure 5b. It is resulted from the enhancement of scattering. Besides, the emission spectra of the sample with varying the concentration of R6G from 0.5 mg mL^{-1} to 6 mg mL^{-1} are shown in Figure S2b. The central wavelength appears red shifts with increasing the concentration of R6G while keeping the concentration of TiO_2 NPs at a fixed value of 0.6 mg mL^{-1}. This may attribute to too more gain material leading to a serious reabsorption.

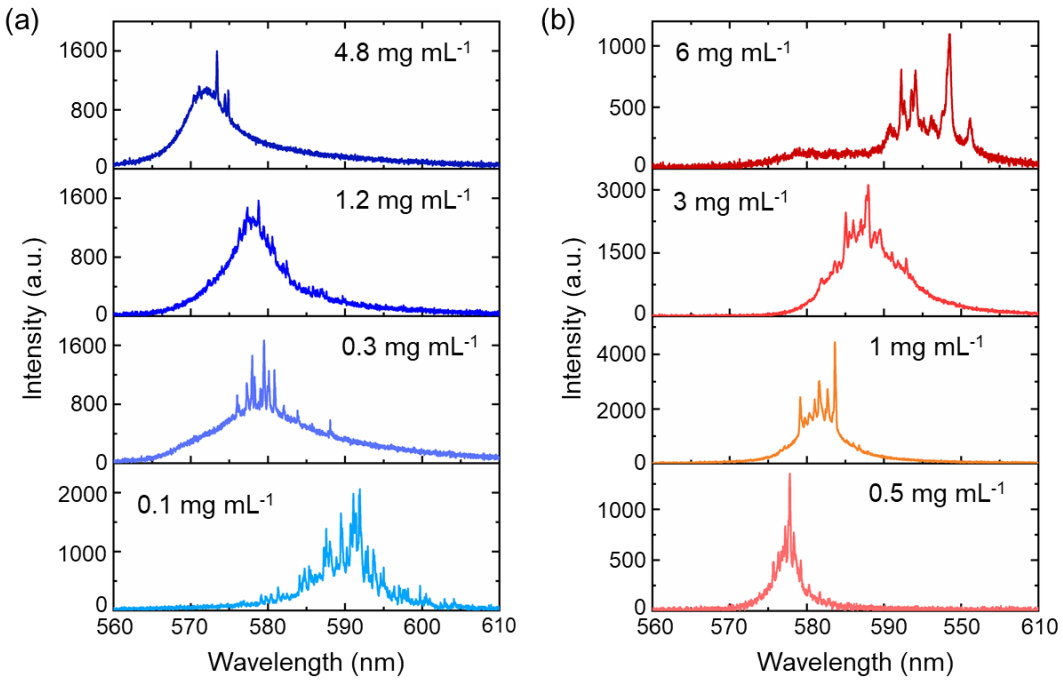

Figure S2. (a) Emission characteristics of the waveguide integrate RL microbelt with different condition of TiO_2 NPs. The emission spectra under different pump power densities. (b) Emission characteristics of the waveguide integrate RL microbelt with different condition of R6G. The emission spectra under different pump power densities.

The corresponding threshold variation with the concentration of R6G and TiO_2 NPs are shown in Figure S3. The thresholds increase firstly and then decrease with increasing the concentration of TiO_2 NPs. In contrast, by increasing the concentration of R6G, the thresholds decrease firstly and then increase.

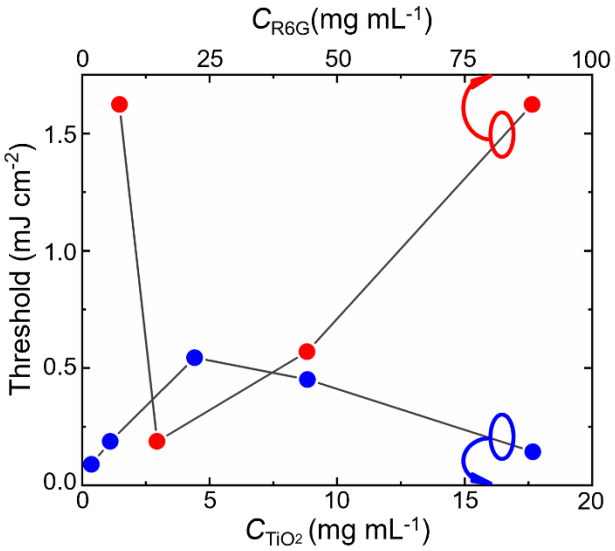

Figure S3. Thresholds variation with the concentration of R6G and TiO_2 NPs.

C: Effect of the width of microbelt on the waveguide integrated RLs

The effect of the microbelt width on the emission of waveguide integrated RLs is studied. When the width of the RL microbelt based on R6G increases from 213.3 μm to 731.7 μm, the number of RL modes (multiple peaks) in the emission spectra increases, as is presented in Figure S4a. This is resulted from the increasing gain molecules, which forms more coherent feedback loops. And because the gain increases, the thresholds decrease with increasing width of RL microbelt (in Figure S4b). And the increasing gain accompanied by reabsorption, resulting to the red shifting of the central wavelength (in Figure S4b).

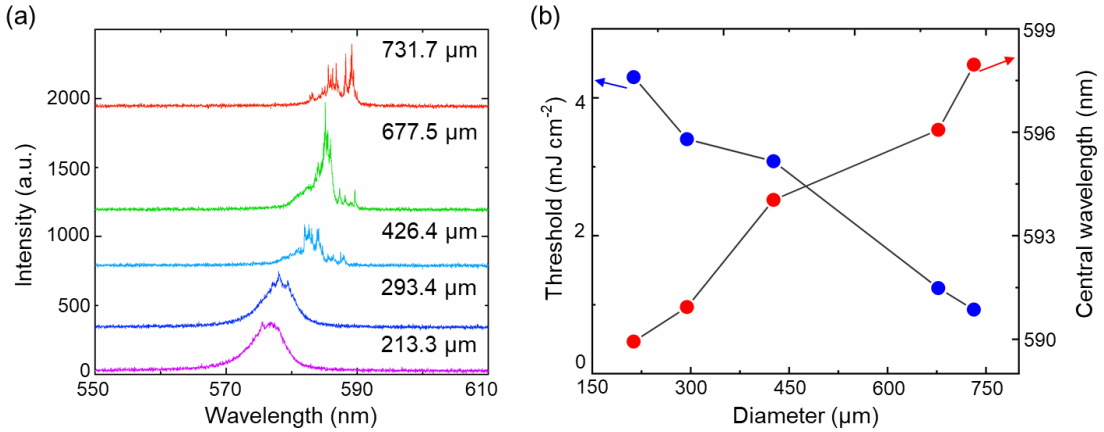

Figure S4. (a) Emission spectra of the waveguide integrate RL microbelt with different microbelt sizes. (b) Thresholds and central wavelength vary with the width of the RL microbelts. The pump energy densities from bottom to top are 12 mJ cm^{-2}, 14 mJ cm^{-2}, 3.9 mJ cm^{-2}, 6.2 mJ cm^{-2}, 2.4. mJ cm^{-2}.

D: Spatial coherence of the waveguide integrated RLs

The spatial coherence of the waveguide-integrated RL is measured based on Yang's double-slit interference, as is presented in Figure S5. As contrast, the interference pattern of traditional lasers (continuous laser at 532 nm) is displayed as stripes of light and dark (in Figure S5a), indicating the good spatial coherence. The spatial coherence of the fiber-integrated RL is measured based on Yang's double-slit interference, which is estimated based on the formula below

$$\gamma = \frac{I_{max} - I_{min}}{I_{max} + I_{min}}$$

And the degree of spatial coherence for traditional lasers is estimated as $\gamma = 0.7344$. The recorded interference pattern presented in Figure S5b shows a uniform distribution of intensity. The degree of spatial coherence is calculated as $\gamma = 0.4260$, which is much lower than that of traditional lasers. The low spatial coherence lasing from the waveguide-integrated RL for imaging systems could improve image quality.

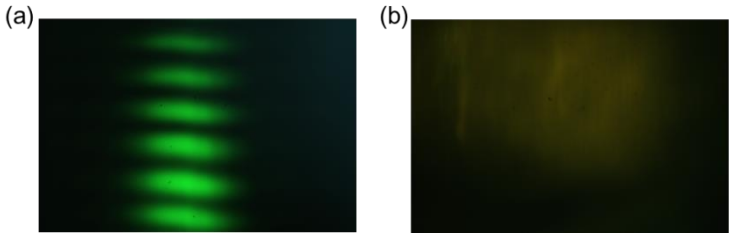

Figure S5. (a) The interference pattern of traditional lasers. (b) The interference pattern of waveguide integrated RL.

E: Effect of the diameter of waveguide on the waveguide integrated RLs

The regime of the lasing from the RL microbelt is studied by changing the diameter of the fiber waveguide on the waveguide integrated RLs. By increasing the diameter of the fiber waveguide, there is no obvious change in the spectra (in Figure S6). And the free spectral range (FSR) also keeps constant with small fluctuations, as the blue dots shown in Figure 2c. However, the FSR for the Whispering Gallery Mode (WGM) resonant decreases with the diameter of cavity [1-2], as the gray dots displayed in Figure S4b. Furthermore, based on the sharp harmonics in power Fourier transform (PFT), equivalent cavities of random laser are estimated. The cavity path length can be calculated by $Lc=d\pi/n$ where n is the refraction index of the random matrix (n=1.5), and d is the position of first peak in PFT spectrum. The calculated cavity lengths are around 53 ± 7 μm. All the results indicate that the regime is random feedback rather than WGM resonant around the fiber.

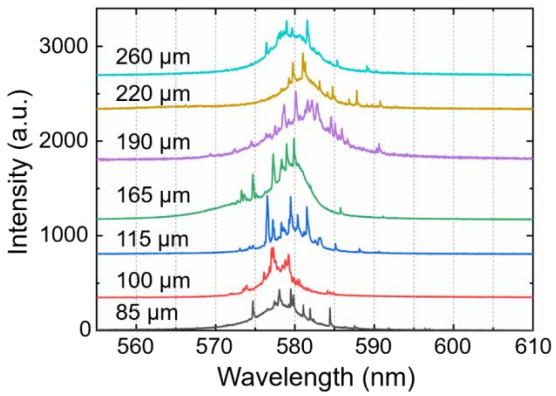

Figure S6. Emission spectra of the waveguide integrate RL microbelt with increasing the diameter of the waveguide fiber. The pump energy density keeps at 7.7 mJ cm^{-2}.

F: Effect of the adjacent RL microbelts on a shared waveguide

To further study the interaction between adjacent RL microbelts on a shared waveguide, we pump the adjacent RL microbelts in different strategy. Two microbelts with different widths are arranged on a fiber. And the pump beam illuminates the microbelts in different ways with pump power density of 4.3 mJ cm^{-2}, as is illustrated

in Figure S7. When the RL microbelt with narrower width is pumped, there is coherent RL spectrum with multiple peaks (RL1). While, When the RL microbelt with wider width is pumped, there emerges similar RL spectrum as the narrow one. The central wavelength red shifts compared the narrow RL microbelt (RL2), which is contributed to the increased gain. Furthermore, when the two RL microbelts are simultaneously pumped, a broad coherent spectrum envelops the spectra of RL1 and RL2, demonstrating there is no interaction between the lasing from RL1 and RL2. In this regard, the light with multiple colors is linear superposition.

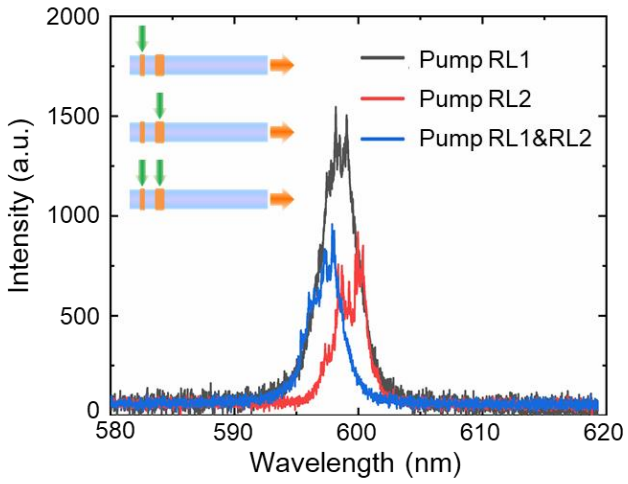

Figure S7. Emission spectra from the waveguide integrated RL microbelts with different pump strategy.

G: Waveguide integrated RLs with different gain and scattering parameter

The influence of waveguide on the emission property of waveguide integrated RLs has been confirmed by changing the fiber to a commercial optical fiber. The emission spectrum of single RL microbelt doped with R6G and TiO_2 NPs on a commercial optical fiber is presented in Figure S8a. For pump energy density at 1.2 mJ cm^{-2}, there is spontaneous emission in the spectrum. As the pump energy density exceeds 1.3 mJ cm^{-2}, initial sharp peaks with sub-nanometer emerge from the broad emission, indicating the building up of random laser. As the pump energy density increases further, the intensity of RL modes increase more rapidly. The RL microbelts with blue-, green- and red-emission can all achieve lasers on the optical fiber, as the bright fiber shown in the photograph inset of Figure S8a. Figure S8b exhibits the threshold behavior for single RL microbelt in Figure S8b, indicating the threshold of random lasing at 1.29 mJ cm^{-2}. The integral emission intensity of waveguide integrated RL by changing detection angle from 0 ºto 180 ºunder a fixed pump condition is plotted in Figure S8c. There is maximum value in the center at the angle of 60 ºand 120 º.

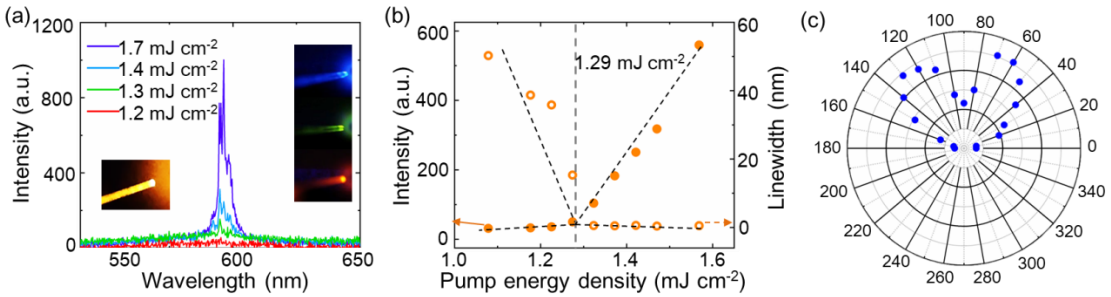

Figure S8. (a) Emission spectra from the waveguide integrated RLs on optical fiber under different pump energy densities. (b) Threshold behavior of the waveguide integrated RLs on optical fiber. (c) Spatial emission property for the waveguide integrated RLs on optical fiber.

The spectra of the waveguide integrated RL with different diameter of the optical fiber are shown in Figure S9a, demonstrating similar phenomenon. And the free spectral range (FSR) keeps unchanged (blue dots in Figure S9b), which is different from that of the WGM laser (gray dots in Figure S9b). The cavity length is measured by power Fourier transform (PFT) spectrum, which is estimated about 38 ± 7 μm (red dots in Figure S9b) as the diameter of waveguide changes from 125 μm to 600 μm. The emission property also does not change with the diameter of the optical fiber, which is similar with the RL microbelt on polymer fiber (in Figure 2c).

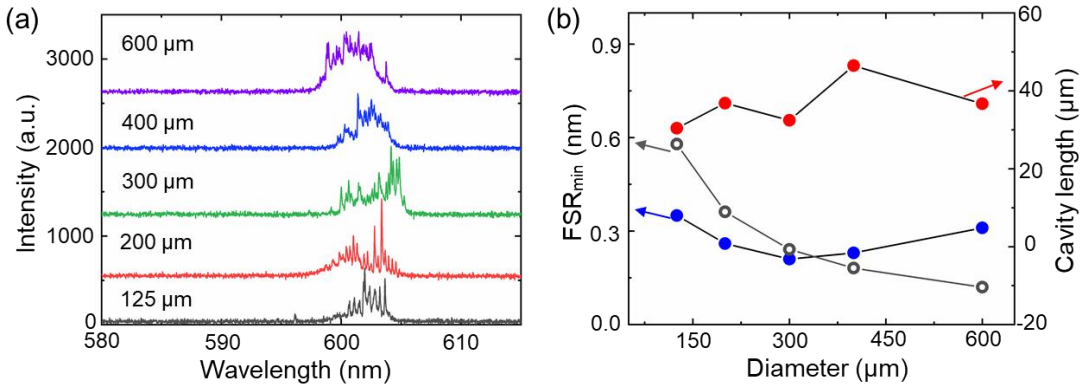

Figure S9. (a) Emission spectra of the waveguide integrate RL on optical fiber with increasing the diameter of the waveguide fiber. (b) FSR and cavity length varies with the width of the diameter of the optical fiber. The pump energy density keeps at 3.71 mJ cm^{-2}.

H: Imaging property under the illumination of RLs on fiber

The imaging property under the illumination of RLs on fiber has been presented in Figure S10a. The RL microbelt on optical fiber is excited and transmitted in the fiber. The emission RL from the end face of the fiber illuminates the inner wall of scallion leaf. The imaging photograph in Figure S10a exhibits structure of the inner wall of scallion leaf. As contrast, the waveguide integrated RL is replaced by a commercial endoscope (MEMONOKB,Y101). The recorded image is presented in Figure S10b, showing similar structure as Figure S10a. This indicates that the waveguide integrated RLs are good sources for long distance imaging. For the medical imaging, the

fiber-integrated RLs with micro-size can detect narrower bio-structures, such as the lining of blood vessels (Figure S10c).

Figure S10. Image of inner wall of scallion leaf taken under (a) the waveguide integrated RL and (b) the commercial endoscope. (c) Schematic illustration of the fiber-integrated RGB RLs as an optional source for high resolution imaging.

References

[1] Gao Z, Wei C, Yan Y, et al. Covert photonic barcodes based on light controlled acidichromism in organic dye doped Whispering-Gallery-Mode microdisks. Adv Mater, 2017, 29: 1701558

[2] Wei C, Gao M, Hu F, et al. Excimer emission in self-assembled organic spherical microstructures: An effective approach to wavelength switchable microlasers. Adv Opt Mater, 2016, 4: 1009-1014